

The WFIRST Coronagraph Instrument Optical Design Update

Hong Tang*, Richard Demers, John Krist, James McGuire, Mayer Rud, Feng Zhao

Jet Propulsion Laboratory, California Institute of Technology, 4800 Oak Grove Drive, Pasadena, CA 91109, USA

ABSTRACT

The WFIRST Coronagraph Instrument will perform direct imaging of exoplanets via coronagraphy of the host star. It uses both the Hybrid Lyot and Shaped Pupil Coronagraphs to meet the mission requirements. The Phase A optical design fits within the allocated instrument enclosure and accommodates both coronagraphic techniques. It also meets the challenging wavefront error requirements. We present the optical performance including throughput of the imaging and IFS channels, as well as the wavefront errors at the first pupil and the imaging channel. We also present polarization effects from optical coatings and analysis of their impacts on the performance of the Hybrid Lyot coronagraph. We report the results of stray light analysis of our Occulting Mask Coronagraph testbed.

Keywords: WFIRST, Coronagraph Instrument, CGI

1. INTRODUCTION

The Wide Field Infrared Survey Telescope (WFIRST) features a Wide Field Instrument (WFI) and a Coronagraph Instrument (CGI) [1]. The current design of the observatory is shown in Figure 1. It is composed of major subsystems and assemblies. They include avionics, communications, solar array and sun-shield, radiators, optical barrel, and the payload. The WFIRST payload consists of the Instrument Carrier (IC), the Imaging Optics Assembly (IOA), and two instruments WFI and CGI. It is illustrated in Figure 2. The IC supports the IOA, WFI and CGI and interfaces with the spacecraft bus. The IOA contains the Optical Telescope Assembly (OTA).

The optical beam train in CGI (in Cycle 5) is composed of three major sub-systems, the Tertiary Collimator Assembly (TCA), Coronagraph, and Integral Field Spectrograph (IFS) [2]. The TCA corrects a large amount of off-axis aberration from the telescope. It also has an extremely low pointing-induced wavefront error response within the limits imposed by the observatory's attitude control system (± 14 mas). In Cycle 6, we decided to directly attach the TCA to the After Metering Structure (AMS) of the telescope. The TCA becomes part of the IOA, providing a stable and collimated interface with the Coronagraph. It also produces an exit pupil at the fast steering mirror (FSM) of the Coronagraph. The new Coronagraph Instrument consists of the Coronagraph Optical Module which includes the optical coronagraph bench, IFS, mechanical, thermal, electrical and control subsystems. The coronagraph bench combines the Hybrid Lyot and Shaped Pupil Coronagraphs (HLC and SPC) into the same optical beam train. It supports either HLC or SPC observation modes by using a series of mask and filter changing mechanisms.

The CGI will perform direct imaging and spectral characterization of known exoplanets over a 480 to 980 nanometer wavelength range in seven bands of 5 to 18% widths. The smallest inner working angle (IWA) of the coronagraph will be $3\lambda/D$ at 506 nm (134 mas) for the HLC mode, and $2.8\lambda/D$ at 660 nm (163 mas) for the SPC mode. The largest outer working angle (OWA) will be approximately $10\lambda/D$ at 575 nm (446 mas) for HLC, and $9\lambda/D$ at 890 nm (706 mas) for SPC. For debris disk imaging with the SPC mode, the IWA will be $6.8\lambda/D$ and the OWA $20\lambda/D$. The complete CGI performance parameters and the filter parameters are published by the Infrared Processing and Analysis Center (IPAC) at the California Institute of Technology [3].

The performance goal for CGI is to achieve a starlight extinction ratio (or contrast) of better than three parts per billion (3×10^{-9}) after post-processing of the speckle pattern over the coronagraph field of view. This should enable the observation of cold Jupiters, and advancement of technologies for proposed future space exoplanets observatories, such as HabEx (the Habitable Exoplanet Imaging Mission) and LUVOIR (the Large UV Optical InfraRed Surveyor). The direct imaging (DI) camera, Nyquist-sampled at 480 nanometers, has a plate scale of 20.8 mas per pixel. A medium

*Hong.Tang@JPL.NASA.GOV

Copyright 2017 California Institute of Technology. Government sponsorship acknowledged.

resolution ($R \sim 50$) integral field spectrograph (IFS) described in reference [4] will produce spectra of the exoplanet in the three contiguous spectral bands that cover the 600 to 980 nanometers range.

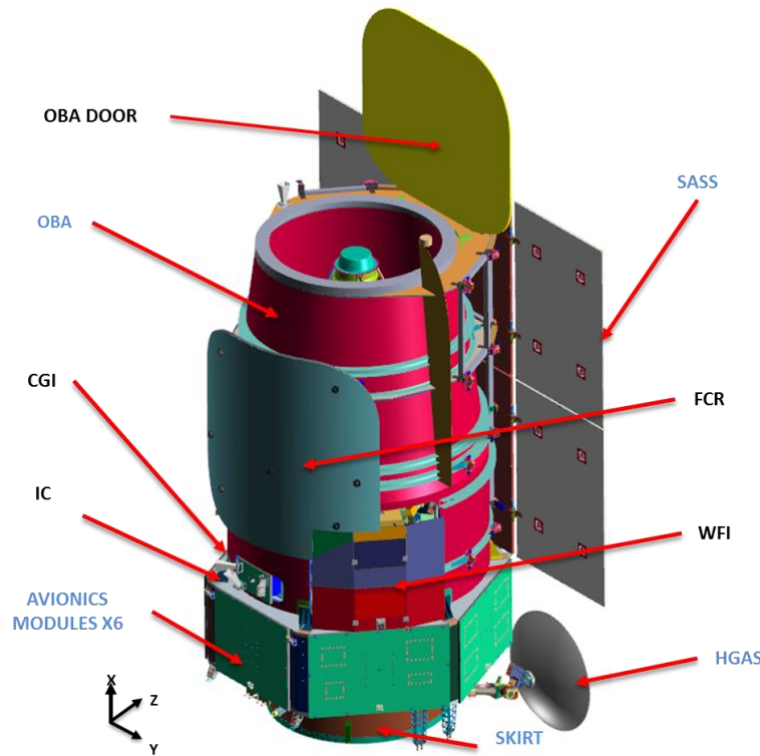


Figure 1. The Wide Field InfraRed Survey Telescope. It is composed of major subsystems: Avionics Modules, High Gain Antenna, Solar Array and Sun Shield, Optical Barrel Assembly, Facility Radiator, Instrument Carrier, Wide-Field Instrument, and Coronagraph Instrument.

We reported on the Cycle 5 optical design of the CGI two years ago at this conference [2]. Here we present updates made in design Cycle 6 and Phase A to the coronagraph instrument. In the following sections, we describe the optical design of the TCA and CGI. We present updates to the polarization imaging capabilities. We also present the results of stray light analysis for the latest testbed for WFIRST coronagraph.

2. OPTICAL DESIGN UPDATE

In design Phase A, the Wide-Field Instrument team decided to directly attach the WFI's tertiary mirror to the OTA. As a result the field of regard of WFI and CGI have changed. The CGI field of regard is 0.4 degree from the telescope optical axis and -120 degree from the +z-axis of the Observatory Coordinate System (OCS). WFI's central field of regard is 0.491 degree from the optical axis and +120 degrees from the +z-axis of OCS. The Instrument Carrier was redesigned to accommodate the change of field position, as shown in Figure 2. One fold mirror was added at the front end to steer light from the OTA to the tertiary mirror inside the TCA. The two instruments have also received new volume allocations. The key and driving requirement for the Phase A CGI optical design was to alter the Cycle 6 design so that it fits into the new volume allocation while still meeting the other requirements, including hosting two coronagraph architectures. We have also improved the imaging channel by adding unpolarized imaging to maximize optical throughput and added two orientations of polarized imaging to reduce uncertainty in determination of the degree of polarization in the imaged light.

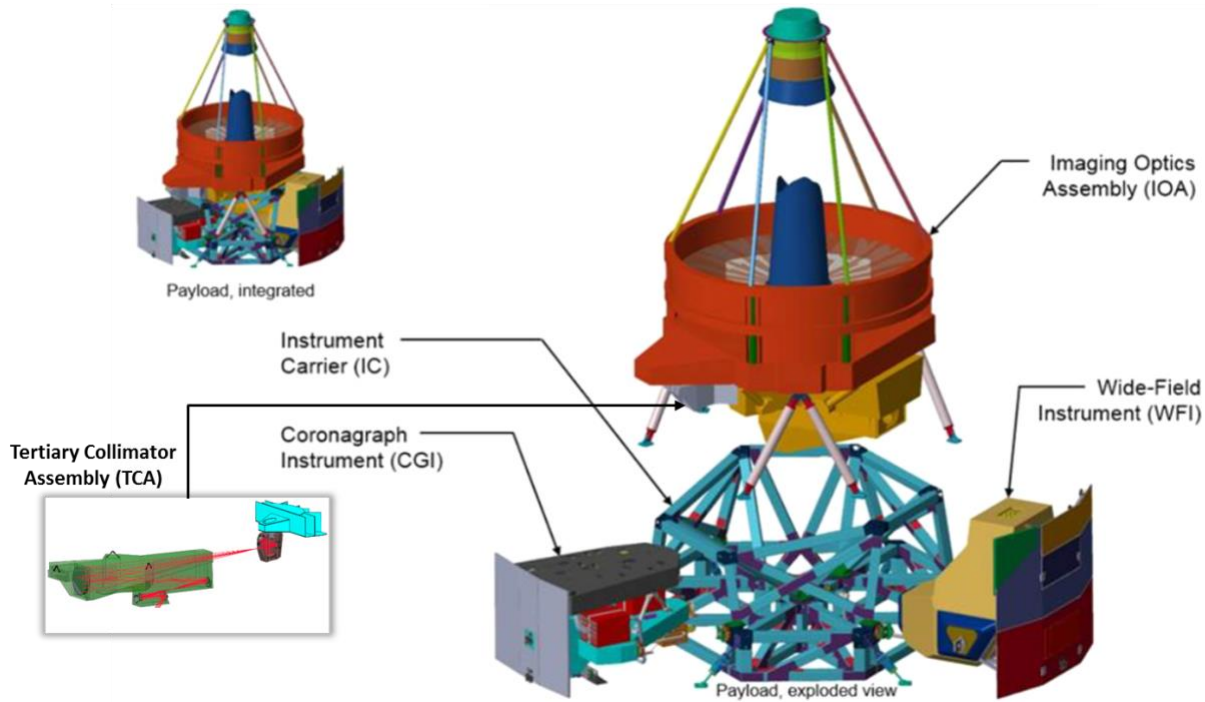


Figure 2. WFIRST Payload contains the Instrument Carrier, Imaging Optics Assembly, Wide-Field Instrument and Coronagraph Instrument.

2.1 Tertiary and Collimator Assembly

The Tertiary and Collimator Assembly (TCA) corrects the coma and astigmatism from the off-axis field location, collimates the beam, and forms an exit pupil at the fast steering mirror inside the CGI. The pick-off mirror assembly directs the light from the telescope toward the tertiary mirror (M3) as shown in Figure 3. We use three mirrors at small angles of incidence to minimize the polarization induced wavefront error (WFE). The tertiary and quaternary (M4) mirrors reduce the 6380 nm root-mean-squared (RMS) WFE from the telescope, down to 7 nm RMS. Furthermore, to minimize the beam walk effects, the WFE variations is constrained to be approximately 10 picometers (RMS) within the line of sight (LOS) change of ± 14 mas per axis, which is the required capability of the observatory attitude control system (ACS).

The performance of the TCA is highly sensitive to any misalignment between the Optical Telescope Assembly (OTA) and TCA. In design Cycle 6, we decided to separate the TCA from CGI and attach the TCA directly to the OTA. In Phase A, we chose to split the TCA into two assemblies, the Pick-Off Mirror Assembly (POMA) and Tertiary Optical Mirror Assembly (TOMA), as shown in Figure 3. The new CGI starts at the fast steering mirror.

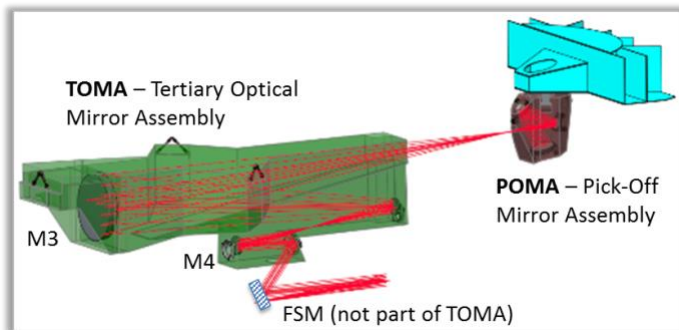


Figure 3. The Tertiary Collimator Assembly is comprised of the pick-off mirrors, the tertiary mirror (M3), the collimator (M4) and two fold mirrors that follow M3 and M4. It is split into the pick-off mirror assembly (POMA) and tertiary optical mirror assembly (TOMA).

The interface between the CGI and the TCA is in the collimated beam so that the sensitivity of WFE to misalignment is reduced by orders of magnitude from Cycle 5, where the TCA was attached to the Instrument Carrier. In Phase A, we reduced the diameter of the exit pupil from 46 mm to 40 mm to accommodate the beam footprint on a heritage FSM. We were also able to push the TCA exit pupil further out to be coplanar with the FSM.

2.3 Polarization Induced Wavefront Error

Light entering an optical system such as the WFIRST telescope linearly polarized states. Light of the two polarizations experiences different amplitude attenuation and phase change when propagating through the optical system. Furthermore, the two polarizations at different points in the pupil experience different amounts of amplitude attenuation and phase change, depending on the thin film coatings applied on mirror surfaces. Light of each input state would retain most energy in its original state and a small amount of energy is coupled into the other state. At the exit pupil of the optical system, there are four polarized wavefronts in the system, the two that are in their original states and the two that coupled into the orthogonal states. With a polarizer we can choose the two wavefronts that are in the same output state. In the CGI, the two DMs work with the coronagraph masks to generate a speckle-suppressed dark field (dark hole) where a faint planet may be detected. We can use a polarizer to optimize the DM's for one polarization to create a deeper dark hole, but we pay the penalty of 50% loss in throughput. We can also choose to optimize the DM's for a dark hole for the average of the two polarizations that may not be as deep, depending on the wavelength band, without paying 50% loss in throughput.

Table 1. Key performance parameters of CGI.

Design Specifications		Value	Unit
WFE (on CGI axis)	After SM	6380	nm (rms)
	After M4	7	
	At FPM	7	
Δ WFE (100 mas off CGI axis)	After M4	30	pm (rms)
Imaging pixel plate scale		0.02	arcsec
Imaging FOV (full)	without masks	10	arcsec
Throughput (R and T)	DI-HLC	0.55	
	DI-SPC	0.51	
	IFS-SPC	0.44	

To model the polarization wavefront error, we decompose the light entering the telescope into -45° and $+45^\circ$ linear polarizations with respect to the Payload coordinate system. The x-z plane is the meridional plane of the OTA and TCA and is formed by the optical axis of OTA and the chief ray of the CGI field. We place a polarizer at the exit pupil of the TCA that can be oriented in either local x or y, where local x is in the meridional plane and perpendicular to the chief ray (local z) at the TCA exit pupil. We have four states of polarized light, $Pol_{X,-45^\circ}$, $Pol_{Y,-45^\circ}$, $Pol_{X,+45^\circ}$, and $Pol_{Y,+45^\circ}$, each with different wavelength-dependent amplitude and phase distributions. The light after the x-polarizer, Pol_x is the incoherent sum of $Pol_{X,-45^\circ}$ and $Pol_{X,+45^\circ}$, so when digging a dark hole in state Pol_x we have to manipulate the sums of intensities and the average of phases. The same applies to Pol_y . In the absence of a polarizer, we have both Pol_x and Pol_y . The DM

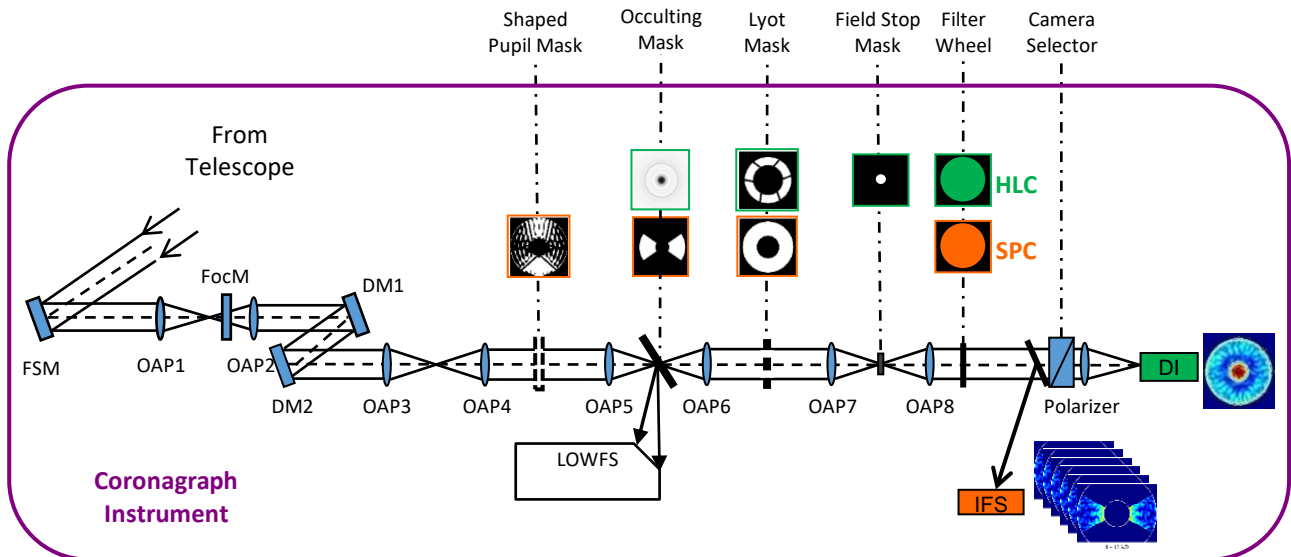


Figure 5. The schematics of CGI. The HLC and SPC mode are achieved with changeable masks. The HLC mode (green) uses the occulting mask, Lyot mask, field mask and color filters. The SPC uses the shaped pupil mask, occulting mask, Lyot mask and color filters. SPC works with IFS and DI channels. The HLC only works with the DI channel.

solutions that for both Pol_x and Pol_y produce shallower depth of a dark hole.

Polarization-Induced Phase Errors: Differences

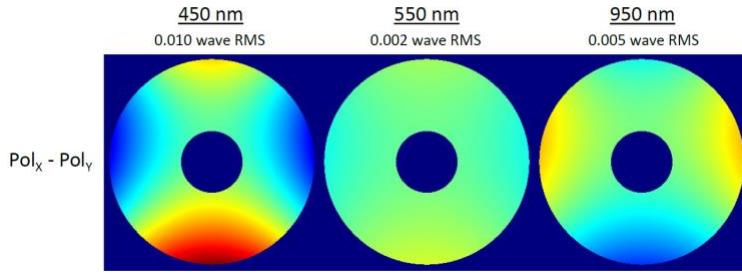


Figure 6. The input to the telescope is decomposed into two linearly polarized states, Pol_{-45°} and Pol_{+45°}, with respect to x-axis. At the exit pupil of TCA, output is measured in two linearly polarized states, Pol_x and Pol_y. The phase in Pol_x is the average of phases from Pol_{x,-45°} and Pol_{x,+45°}. The difference in phases of the two states, Pol_x – Pol_y, is plotted here for three wavelengths.

hole in one image or slightly shallower dark holes in both images. Recent analysis shows that in the presence of LOS jitter the differences in depth between single and dual polarization dark holes decreases [7,8]. Thus, we added an unpolarized imaging mode in Phase A that provides sufficient contrast and ~2x gain in throughput.

2.4 Direct Imaging Channel

We removed the Wollaston prism in the direct imaging (DI) channel to accommodate unpolarized imaging. We added four imaging lenses with linear polarizers of different orientation for polarized imaging. All polarizer and lens combinations are mounted in the last wheel, shown in Figure 7. With a Wollaston prism, light in the DI channel is permanently split into 0 and 90 polarization mode. In the new scheme, four polarized mode enables higher certainty in measuring the degree of polarization of the light at DI camera. The wheel mechanism also contains pupil imaging lens, four phase-retrieval lenses and the IFS Select mirror.

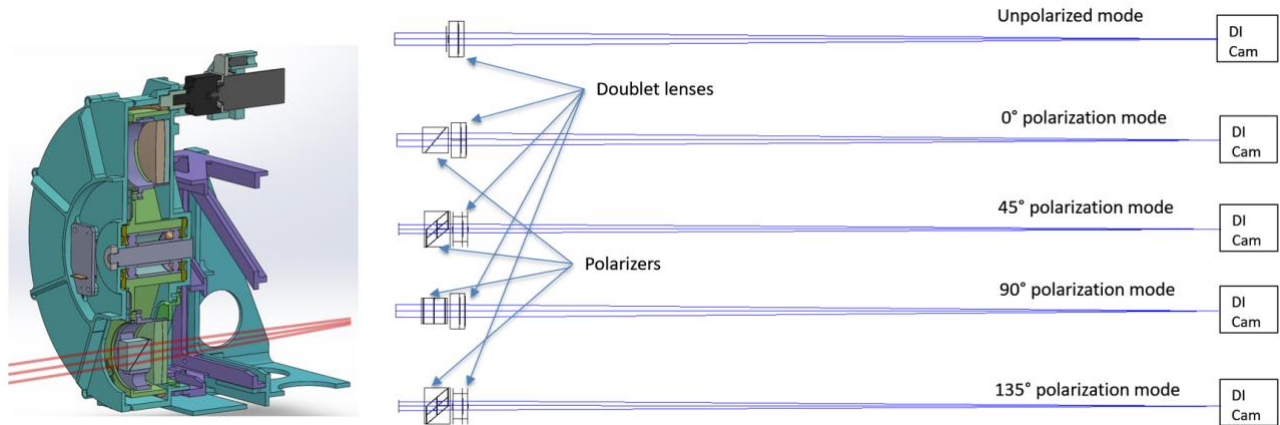


Figure 7. The direct imaging channel has new capabilities to form unpolarized imaging on the DI camera. It can also form polarized image of four orientations.

2.5 Stray light analysis for the OMC testbed

Stray light analysis of the Occulting Mask Coronagraph Testbed (OMC) was carried out by Photon Engineering, Inc. under contract with the Jet Propulsion Laboratory [9]. The OMC optical layout is based on the Cycle 5 design. In the initial analysis, we considered only the stray light from the on-axis source that is scattered by optical surfaces due to surface micro roughness. The assumptions for stray light analysis are listed in Figure 8(a). The surface scattering follows the Harvey-Shack model [10]. The BDSF (Bi-directional Scattering Distribution Function) is rendered in the plane of incidence in Figure 8(b). At the detector (DI Camera) plane, a mask of 2.5 mm diameter is applied, which equals to 40

Figure 6 shows the differential phase between Pol_x and Pol_y [7]. It is significantly smaller near 550 nm due to the characteristics of the reflective coatings on all the mirrors. From there it increases slowly towards longer wavelengths and faster towards shorter ones. In design Phase A, the shortest band was moved long-wards to 505 nm. It is a 10% band, so the shortest wavelength of CGI is 480 nm.

In Cycle 5 and Cycle 6 we used a Wollaston prism to split the x and y polarizations to form two images simultaneously on the direct imaging camera. We could choose to optimize the DM's to have a deeper dark

λ/D at 550 nm. Light outside the mask is ignored in the analysis. The total scattered light that reaches the detector has an average irradiance of 8.35×10^{-9} (Watt/mm²). This seems high for a coronagraph system to deal with. Upon examination of the optical path difference (OPD) of the scattered light from that of the on-axis specular light, almost all the scattered light has OPD less than $5.5 \mu\text{m}$, which is the coherence length of light at the central wavelength of 550 nm with a bandwidth of 10%. Hence, we separate the scattered light into two categories, OPD less than $5.5 \mu\text{m}$ and OPD greater than $5.5 \mu\text{m}$. The average irradiance values of the two categories are shown in Figure 8(c) and (d). The former is considered to be “coherent” and can be controlled by the DM’s. The latter is considered the true stray light that just adds to the background on the detector. It has an average irradiance of 2.85×10^{-15} (Watt/mm²), which is much smaller. To estimate the effect of the stray light to the contrast, we take the ratio of the irradiance from the stray light to the peak irradiance of the point spread function (PSF) with the occulter out of the path. The peak irradiance without the occulter is 0.055 (Watt/mm²). Thus, the estimated contrast of the incoherent scattered-light due to the surface micro roughness is 5.2×10^{-14} . The value is orders of magnitude lower than the contrast that we had achieved in the OMC testbed, 1.6×10^{-9} . We can conclude that the stray light from optical surface scattering is not a significant contributor to the incoherent background observed in the OMC testbed.

We plan to carry out stray light analysis of the CGI optical path with the full OTA and TCA model in Phase A. We will include light from the star under observation and other stellar objects in the larger field of view of the OTA and examine the irradiance level of all the sources at the DI camera, LOWFS camera and IFS camera.

- All optical surfaces use a Harvey-Shack BSDF model to represent scatter due to RMS micro-roughness
- DMs: RMS = 39 Angstroms
- Flats: RMS = 10 Angstroms
- OAPs: RMS = 15 Angstroms
- OTA mirrors: RMS = 20 Angstroms
- Lenses and windows: RMS = 20 Angstroms
- All surfaces are pristine, no contamination models have been applied
- Mask surfaces are treated as perfect absorbers

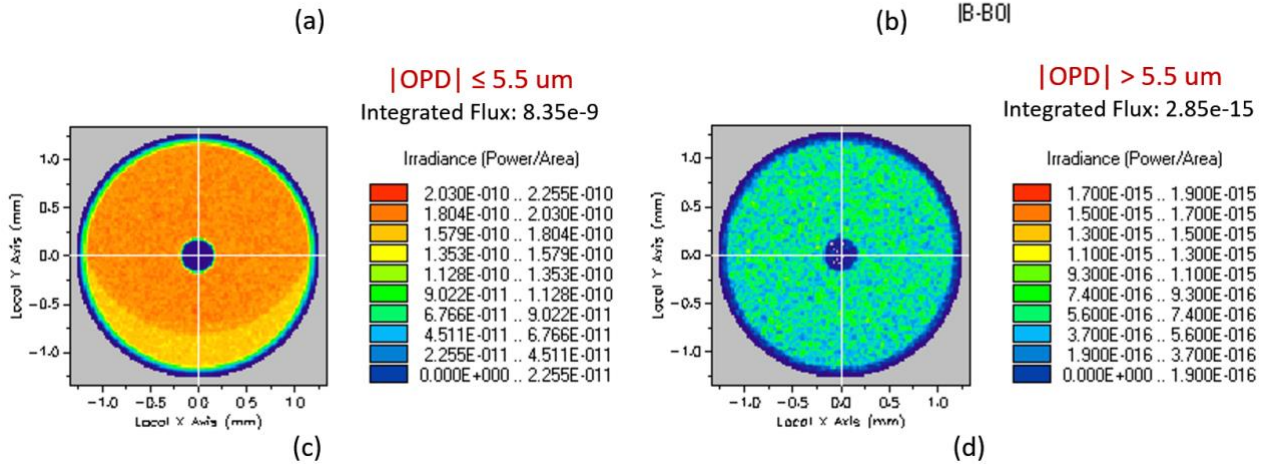
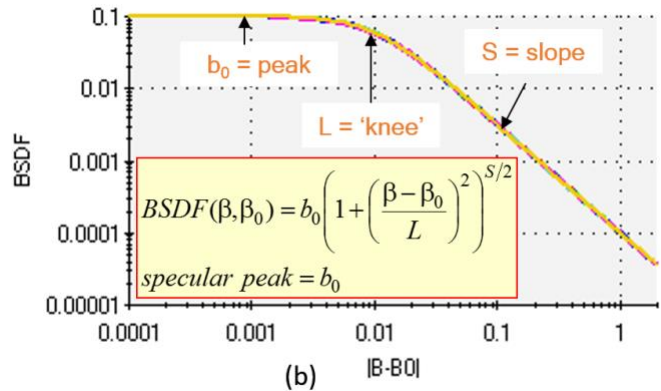


Figure 8. The assumptions and results from initial stray light analysis of the OMC testbed. We assume that the scattering due surface micro roughness follow Harvey-Shack model. The in-plane BSDF is show in (b). Quantities $\beta = \sin(\theta)$ and $\beta_0 = \sin(\theta_0)$, where θ is the scattering angle and θ_0 is the angle of incidence. We separated the scattered light into “coherent” and “incoherent” parts. The “coherent” part (c) has optical path difference from that of the on-axis specular path less than $5.5 \mu\text{m}$, which is the coherence length of light at 550 nm with a bandwidth of 55 nm. With the coronagraph occulter in the path, light at the center (specular) is blocked.

3. ACKNOWLEDGMENTS

The research described in this presentation was performed at the Jet Propulsion Laboratory of the California Institute of Technology, under contract with the National Aeronautics and Space Administration, in close collaboration with the WFIRST project teams at the NASA Goddard Space Flight Center and Harris Corporation.

REFERENCES

1. Wide-Field Infrared Survey Telescope (WFIRST) – NASA, <https://wfirst.gsfc.nasa.gov/>.
2. H. Tang, et al, “The WFIRST/AFTA Coronagraph Instrument Optical Design”, Proc. SPIE 9605 (2015).
3. Spacecraft and Instrument Parameters – IPAC WFIRST, https://wfirst.ipac.caltech.edu/sims/Param_db.html.
4. Q. Gong, et al, “Flight Integral Field Spectrograph (IFS) Optical design for WFIRST Coronagraphic Exoplanet Demonstration”, Proc. SPIE 10400 (2017).
5. F. Shi, et al, “Dynamic Testbed Demonstration of WFIRST Coronagraph Low Order Wavefront Sensing and Control (LOWFS/C)”, Proc. SPIE 10400 (2017).
6. Q. Gong, et al, “Prototype Imaging Spectrograph for Coronagraphic Exoplanet Studies (PISCES) for WFIRST-AFTA”, Proc. SPIE 9605 (2015).
7. J. Krist, “Is WFIRST Coronagraph Polarization Splitting Really Needed? Polarization Effect vs Wavelength & Jitter”, Internal Communication, Jet Propulsion Laboratory, December 6, 2016.
8. J. Krist, et al, “WFIRST coronagraph optical modeling”, Proc. SPIE 10400 (2017).
9. S. Ellis, “OMC Testbed Stray Light Analysis Final Report – Rev A”, Report to Jet Propulsion Laboratory, Photon Engineering, November 10, 2016.
10. J. Harvey, “Light-Scattering Characteristics of Optical Surfaces”, Ph.D. Dissertation, University of Arizona (1976).